





Open Archive Toulouse Archive Ouverte

OATAO is an open access repository that collects the work of Toulouse researchers and makes it freely available over the web where possible

This is an author's version published in: <http://oatao.univ-toulouse.fr/28752>

Official URL:

To cite this version: Alazard, Daniel  and Cumer, Christelle and Sanfedino, Francesco  and Oddenino, Davide and Brugnoli, Andrea *Characterization of sadm induced disturbances and their effects on spacecraft pointing errors.* (2021) In: 11th International ESA Conference on Guidance, Navigation & Control Systems (ESA GNC), 22 June 2021 - 25 June 2021 (Netherlands).

Any correspondence concerning this service should be sent to the repository administrator: tech-oatao@listes-diff.inp-toulouse.fr

CHARACTERIZATION OF SADM INDUCED DISTURBANCES AND THEIR EFFECTS ON SPACECRAFT POINTING ERRORS

Daniel Alazard⁽¹⁾, Christelle Cumer⁽²⁾, Francesco Sanfedino⁽¹⁾, Davide Oddenino⁽³⁾, Andréa Brugnoli⁽¹⁾

^{(1),(3)} *University of Toulouse, ISAE-SUPAERO, 10 Avenue Edouard Belin, BP-54032, 31055 Toulouse Cedex 4, France, +33 (0)561338094, daniel.alazard@isae.fr, francesco.sanfedino@isae.fr, andrea.brugnoli@isae.fr*

⁽²⁾ *Onera, 2 Avenue Edouard Belin, 31055 Toulouse Cedex 4, France, +33 (0)562252563, christelle.cumer@onera.com*

⁽⁴⁾ *ESA/ESTEC, Keplerlaan 1, 2201 AZ Noordwijk, The Netherlands, +31 715654367, davide.oddnino@esa.int*

ABSTRACT

This paper presents the modeling and analysis of the induced oscillations due to the Solar Array Drive Mechanism (SADM) on the pointing performances of a generic Earth observation spacecraft. First the SDT (Satellite Dynamics Toolbox) is used to obtain a Linear Parameter Varying model of the spacecraft fitted with a flexible solar panel parameterized according to its angular configuration. Then a detailed model of the SADM including the stepper motor and the gear box is included using the TITOP (Two-Input Two-Output Ports) approach. Such an approach allows to build the dynamic model of the structure just by assembling the sub-structure models. TITOP models consider the 6 d.o.f. (degrees of freedom) to take into account all the geometrical, kinematic and dynamic couplings required to capture the propagation of the perturbations inside the overall flexible structure. Moreover these models allow the user to evaluate the pointing errors on the 3 axes. Parametric robustness analysis tools are then used to isolate the worst harmonics of the various SADM imperfections and the solar array angular configuration from the pointing performance point of view.

1 INTRODUCTION

Among spacecraft internal disturbance sources, the imperfections on the SADM contribute significantly to the overall spacecraft pointing error budget [1, 2]. These imperfections create harmonic disturbing torques when the solar array is driven at a constant angular rate and they are due to: (i) the micro steps in the stepper motor operating mode, (ii) the potential imperfections in the gear pair contacts inside the gearbox commonly used between the stepper motor and the solar array. These harmonic disturbances can be magnified considering the flexible modes of the solar panels which induce resonances in the dynamic model of the whole spacecraft. These resonance frequencies and magnitudes depend on the mass/inertia ratios between the spacecraft main body and the solar array. Moreover these mass/inertia ratios depend also on the angular configuration of the solar array with respect to the main body and require to consider the 3 attitudes degrees-of-freedom simultaneously.

From the modeling point of view, the challenge consists in deriving the required model in order to capture just the dynamic interactions on the 3 axes between:

- the SADM which requires a detailed and accurate model, including harmonic disturbances, located at the connection point between the spacecraft main body and the solar array,
- the flexible modes of the overall spacecraft structure, which requires a sub-structured modeling approach and which depends both on the angular configuration of the solar array and on the attitude control system.

Starting from the Satellite Dynamic Toolbox (SDT) User Guide [3], this paper summarizes the equations and the TITOP models which will be used to take into account the SADM in the overall spacecraft model developed with the SDT.

The SADM model is composed of a stepper motor and a gear box. A stepper motor model is described in [4] and [2]. In [2], the proposed model is a simulation model and takes also into account the electronic part used to control the stepper motor. This part is highly non-linear and is not considered here where the objective is to derive a model for analysis purpose (rather than a pure simulation) which could be used during preliminary design phase. The model described in [4] focuses on the electro-mechanical behavior of the stepper model and is suitable for analysis in the linear domain.

The gearbox TITOP model includes also a disturbance input whose harmonic content is derived thanks to an accurate kinematic model. This kinematic model [5, 6], previously developed for the power transmission gear box of an helicopter rotor, provides the list of all the fundamental frequencies of the various imperfections that can appear in contact pairs of a gear mechanism.

This paper is organized as follows. In section 2, a summary on the SDT and TITOP models, seen as tools for flexible-multi-body system modeling, is presented. Section 3 details the TITOP model of a SADM with the two components: the stepper motor and the gear box, including the internal torque disturbances. Sections 4 and 5 present the application on a generic Earth observation spacecraft where recorded telemetries highlight some oscillations on the pointing errors with magnitudes varying according the solar array angular configuration. More particularly: the results of the worst case analysis are presented in Section 4 and the simulation model with time-domain analysis are presented in Section 5. Conclusion and perspectives are provided in Section 6.

The results presented in this paper have been achieved under funding by the ESA TDE programme with contract 4000122779/18/NL/GCL. The view expressed in this paper can in no way be taken to reflect the official opinion of the European Space Agency.)

2 BACKGROUND ON FLEXIBLE-MULTI-BODY SYSTEMS DYNAMICS

2.1 Summary of the SDT

The objective is to compute the inverse dynamic model, that is the relation between the 6 components of the wrench $\mathbf{W}_{ext,B} = [\mathbf{F}_{ext}^T \quad \mathbf{T}_{ext,B}^T]^T$ of the resulting external force and torque applied to the satellite at its center of mass B (input) and the 6 components of the acceleration twist $\dot{\mathbf{x}}_B = [\mathbf{a}_B^T \quad \dot{\boldsymbol{\omega}}^T]^T$ of point B (output). The satellite is assumed to be composed of a rigid main body or base \mathcal{B} with one or several flexible appendages \mathcal{A}_i connected to the base at points P_i . The model can also take into account a revolute joint at the point P_i between the appendage and the main body. Then the 6×6

inverse dynamic model is augmented by a new channel corresponding to the transfer between C_{m_i} , the torque applied around the joint axis by a mechanism (for instance the SADM) and the relative angular acceleration $\ddot{\theta}_i$ inside the joint. In the case of a single appendage \mathcal{A} , the block diagram representation of this model is depicted in Figure 1 where (see [3], for a detailed nomenclature):

- $[\mathbf{D}_B^{\mathcal{B}}]_{\mathcal{R}_b} = \begin{bmatrix} m^{\mathcal{B}}\mathbf{I}_3 & \mathbf{0}_{3 \times 3} \\ \mathbf{0}_{3 \times 3} & [\mathbf{I}_B^{\mathcal{B}}]_{\mathcal{R}_b} \end{bmatrix}$,
- $[\mathbf{M}_P^{\mathcal{A}}]_{\mathcal{R}_a}(s) = \begin{bmatrix} & & & & & & \\ & & & & & & \\ & & & & & & \\ & & & & & & \\ 0 & 0 & 0 & x_{r_a} & y_{r_a} & z_{r_a} & \\ & & & & & & \end{bmatrix} [\mathbf{D}_P^{\mathcal{A}}]_{\mathcal{R}_a}(s) \begin{bmatrix} 0 \\ 0 \\ 0 \\ \mathbf{I}_6 \\ x_{r_a} \\ y_{r_a} \\ z_{r_a} \end{bmatrix}$ (A is the center of mass of body \mathcal{A} and $[\mathbf{r}_a]_{\mathcal{R}_a} = [x_{r_a}, y_{r_a}, z_{r_a}]^T$ is a unit vector along the revolute joint axis expressed in the body \mathcal{A} frame \mathcal{R}_a),
- $[\mathbf{D}_P^{\mathcal{A}}]_{\mathcal{R}_a}(s) = [\mathbf{D}_P^{\mathcal{A}}]_{\mathcal{R}_a} - \sum_{i=1}^N \mathbf{I}_{i,P}^T \mathbf{I}_{i,P} \frac{s^2}{s^2 + 2\xi_i \omega_i s + \omega_i^2}$ ($\mathbf{I}_{i,P}$, ω_i , ξ_i are, respectively: the modal participation factors at point P , the frequencies and the damping ratios of the N flexible modes of body \mathcal{A}),
- $[\mathbf{D}_P^{\mathcal{A}}]_{\mathcal{R}_a} = [\boldsymbol{\tau}_{AP}]_{\mathcal{R}_a}^T \begin{bmatrix} m^{\mathcal{A}}\mathbf{I}_3 & \mathbf{0}_{3 \times 3} \\ \mathbf{0}_{3 \times 3} & [\mathbf{I}_A^{\mathcal{A}}]_{\mathcal{R}_a} \end{bmatrix} [\boldsymbol{\tau}_{AP}]_{\mathcal{R}_a}$ ($\boldsymbol{\tau}_{AP}$ is the kinematic model between points A and P),
- the notation $[\mathbf{M}_P^{\mathcal{A}}]_{\mathcal{R}_a}^{-17}(s)$ stands for the inversion of the 7-th channel in the system $[\mathbf{M}_P^{\mathcal{A}}]_{\mathcal{R}_a}(s)$ (see also [7]),
- $\mathbf{P}_{a/b}$ is the Direction Cosine Matrix (DCM) of the rotation from frame \mathcal{R}_b to frame \mathcal{R}_a .

Finally,

- the inverse dynamic model $[\mathbf{M}_B^{\mathcal{B}+\mathcal{A}}]_{\mathcal{R}_b}^{-1}(s)$ of the assembled $\mathcal{B} + \mathcal{A}$ can be transported to any reference point O of the main body \mathcal{B} (then denoted $[\mathbf{M}_O^{\mathcal{B}+\mathcal{A}}]_{\mathcal{R}_b}^{-1}(s)$),
- the obtained model can be parameterized according to

$$\sigma_4 = \tan \frac{\theta}{4}$$

where θ is the angular configuration (in radian) of the revolute joint [8, 9] (see also appendix). Such a model, denoted as $[\mathbf{M}_O^{\mathcal{B}+\mathcal{A}}]_{\mathcal{R}_b}^{-1}(s, \sigma_4)$ is an LPV (Linear Parametric Variant) model valid for a whole revolution of the appendage ($\theta \in [-\pi, +\pi]$ or $\sigma_4 \in [-1, 1]$) and is fully compatible with the tools of the MATLAB[®] Robust Control Toolbox.

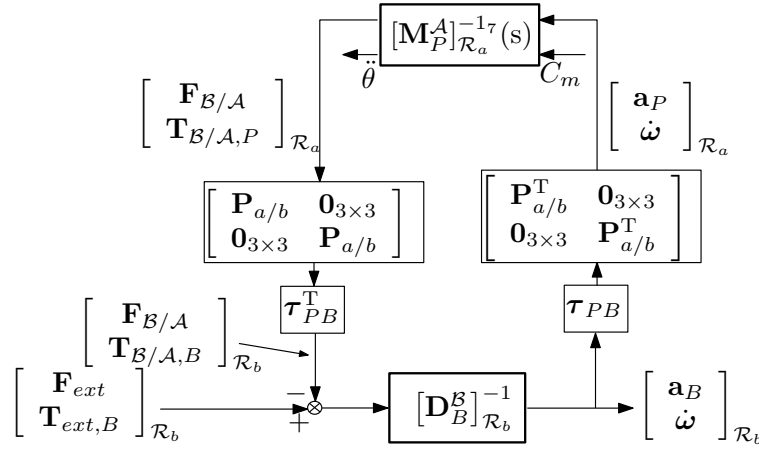


Figure 1: The block diagram representation of the inverse dynamic model $[\mathbf{M}_B^{\mathcal{B}+\mathcal{A}}]_{\mathcal{R}_b}^{-1}(s)$ of the system composed of a main body \mathcal{B} with a flexible appendage \mathcal{A} connected to the main body at the point P through a revolute joint. C_m is the driving torque around the joint axis. $\ddot{\theta}$ is the angular acceleration inside the joint.

2.2 Summary of the TITOP model approach

The TITOP model approach extends the previous framework to any kind of open kinematics chain (or tree-like structure) of flexible bodies; i.e. systems where an intermediate body can be flexible. In the previous approach, flexible bodies can only be located at the ends of the chain (as the leaves of the tree-like structure).

The flexible substructure \mathcal{A} connected to the parent substructure \mathcal{P} at the point P and to the child substructure \mathcal{C} at point C is depicted in Fig. 2. The double-port or TITOP (Two-Input Two-Output Port) model $\mathbf{D}_{P,C}^{\mathcal{A}}(s)$, proposed in [7, 10], is a linear dynamic model between 12 inputs:

- the 6 components in \mathcal{R}_a of the wrench $\mathbf{W}_{C/A,C} = \begin{bmatrix} \mathbf{F}_{C/A} \\ \mathbf{T}_{C/A,C} \end{bmatrix}$ applied by the child substructure \mathcal{C} to \mathcal{A} at point C ,
- the 6 components in \mathcal{R}_a of the acceleration twist $\ddot{\mathbf{x}}_P = \begin{bmatrix} \mathbf{a}_P \\ \dot{\boldsymbol{\omega}}_P \end{bmatrix}$ (time-derivative of the twist) of point P ,

and 12 outputs:

- the 6 components in \mathcal{R}_a of the acceleration twist $\ddot{\mathbf{x}}_C = \begin{bmatrix} \mathbf{a}_C \\ \dot{\boldsymbol{\omega}}_C \end{bmatrix}$ of point C ,
- the 6 components in \mathcal{R}_a of the wrench $\mathbf{W}_{A/P,P} = \begin{bmatrix} \mathbf{F}_{A/P} \\ \mathbf{T}_{A/P,P} \end{bmatrix}$ applied by \mathcal{A} to the parent substructure \mathcal{P} at point P ,

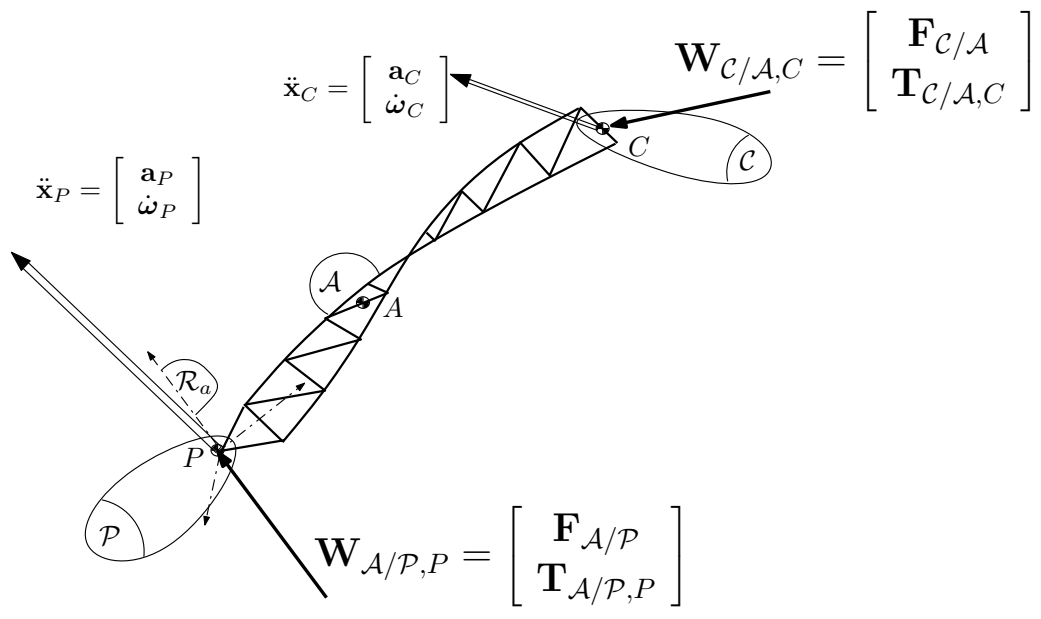


Figure 2: The flexible sub-structure \mathcal{A} in the structure.

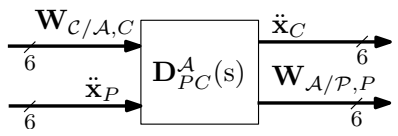


Figure 3: Block-diagram of the TITOP model $\mathbf{D}_{PC}^A(s)$ of \mathcal{A} .

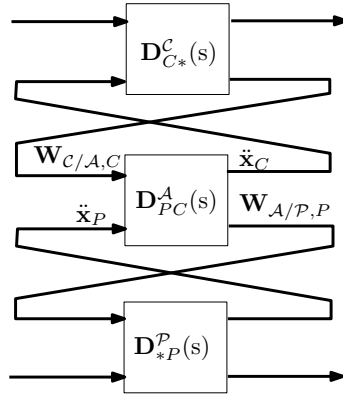


Figure 4: Connection of the substructures \mathcal{P} , \mathcal{A} , \mathcal{C} .

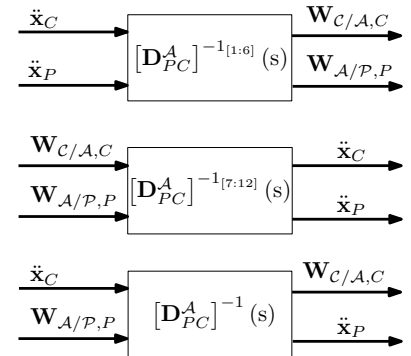
and can be represented by the block-diagram depicted in Fig. 3.

The state space representation of such a TITOP model $\mathbf{D}_{P,C}^A(s)$ is detailed in [10] and involves data (frequencies ω_i , damping ratios ξ_i , modal participation factors $\mathbf{l}_{i,p}$ at point P , modal shapes $\varphi_{i,C}$ at point C of the flexible modes and the kinematic model τ_{CP}) which can be directly read in the NASTRAN[®]/PATRAN[®] analysis output files when the sub-structure \mathcal{A} is clamped at point P and free at point C . The TITOP model embeds, in the same minimal state-space realization, the direct dynamic model (transfer from acceleration to force) of the substructure \mathcal{A} at the point P and the inverse dynamic model (transfer from force to acceleration) of \mathcal{A} at the point C .

The connection of \mathcal{A} to the parent substructure \mathcal{P} at point P and the child substructure \mathcal{C} at point C can be modeled just by feedback connections of the TITOP models of the various sub-structures according to Fig. 4.

Furthermore, $[\mathbf{D}_{P,C}^A]^{-1\mathbf{I}}(s)$ denotes the model where the channels numbered in the index vector \mathbf{I} are inverted (according to the procedure described in [7]). This channel inversion operation is very useful to analyze the dynamics of the link \mathcal{A} for various boundary conditions:

- clamped at P and clamped at C :
- free at P and free at C :
- free at P and clamped at C :



The TITOP model of a beam was used in [11] to co-design the attitude control laws and the boom linking the deployable reflector to the main body. An extension to NINOP (N -port model) was proposed in [2, 12] to model a solar array composed of several panels. Channel inversion operation can be used to model closed kinematics chain of flexible bodies as it was highlighted in [7] on the four bar mechanism.

3 TITOP MODEL OF THE SADM

The TITOP approach is used here to model the SADM. Although this mechanism is located at a particular point in the structure, this approach is suitable:

- to propagate the 6 d.o.f wrench and twist from each input/output side of the SADM, between the solar panel \mathcal{A} and the main body \mathcal{B} ,
- to set the stator of the stepper motor or the gearbox frame on a moving body (that is not the case in [4]),
- to add additional inputs in order to consider the internal disturbing torque and its transmission to the entire spacecraft structure.

The SADM is composed of two main elements: the stepper motor, referenced as body r and the gearbox, referenced as body g .

3.1 TITOP model $M^r(s)$ of the stepper motor

Following [4], the stepper motor inside the revolute joint is characterized by the set of parameters depicted in Table 1. The model proposed in [4] is adapted here to take into account that the stepper

parameter	description	unity
z	rotor teeth number	.
p	beat number	.
n	subdivision number (μ -steps)	.
I	amplitude of the two-phase current	A
J_r	rotor inertia	$Kg\ m^2$
K_m	motor torque constant	$Nm/A/rd$
C_0	viscous damping coefficient	Nms/rd

Table 1: Characteristic parameters of a bi-polar stepper motor.

motor stator is hold by the main body \mathcal{B} with an inertial angular acceleration $\dot{\omega}$. The inertial angular acceleration of the stepper motor stator and rotor are respectively denoted $\dot{\omega}_{in}$, $\dot{\omega}_{out}$. θ is the relative angular configuration of the rotor w.r.t. the stator. The unit vector along the mechanism axis is \mathbf{r}_a . Thus, an intermediate frame \mathcal{R}_r attached to the motor is defined such that its third-axis is aligned with \mathbf{r}_a . In the following description the inputs and the outputs of the TITOP model $M^r(s)$ are expressed in the appendage frame \mathcal{R}_a . The DCM from frame \mathcal{R}_r to frame \mathcal{R}_a is defined as:

$$\mathbf{P}_{r/a} = \mathbf{P}_{r_a} \begin{bmatrix} \det(\mathbf{P}_{r_a}) & 0 & 0 \\ 0 & 1 & 0 \\ 0 & 0 & 1 \end{bmatrix}, \text{ with: } \mathbf{P}_{r_a} = [\text{null}([\mathbf{r}_a]_{\mathcal{R}_a}^T) \quad [\mathbf{r}_a]_{\mathcal{R}_a}].$$

Then the stepper motor TITOP model is described by the following equations or by the block-diagram depicted in Figure 6:

- $J_r(\ddot{\theta} + [\mathbf{r}_a]_{\mathcal{R}_a}^T [\dot{\boldsymbol{\omega}}_{in}]_{\mathcal{R}_a}) = C_m + \underbrace{[\mathbf{r}_a]_{\mathcal{R}_a}^T [\mathbf{T}_{A/r,P}]_{\mathcal{R}_a}}_{-C_l}$ where C_m and C_l are respectively the driving torque and the torque applied to the load (the solar array) along the mechanism axis,
- $C_m = K_m I \gamma i - C_0 \dot{\theta} - K_0 \theta$ with:
 - $K_0 = K_m I z$ (Nm/rd) is the electromagnetic stiffness,
 - $\gamma = \frac{2\pi}{pn}$ (rd) is the electrical μ -step angle,
 - i (integer) is the current μ -step number.

i is the input signal of this model and it can be computed by:

$$i = \text{floor}(\theta_{ref}/\alpha) = \text{floor}(\dot{\theta}_{ref} t/\alpha) .$$

where

- $\alpha = \frac{2\pi}{zpn}$ (rd) is the mechanical μ -step angle,
- t (s) is the time.

The stair-shape integer input signal $i(t)$ can be generated by the following process described in Figure 5 in order to track a given reference input on the angular rate $\dot{\theta}_{ref}$,

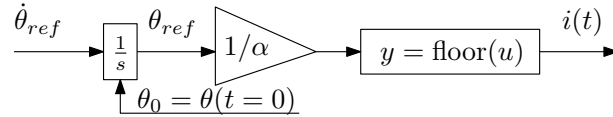


Figure 5: Generator process for $i(t)$.

- $\dot{\boldsymbol{\omega}}_{in} = \dot{\boldsymbol{\omega}}$,
- $\dot{\boldsymbol{\omega}}_{out} = \dot{\boldsymbol{\omega}}_{in} + \ddot{\theta}$,
- $\mathbf{F}_{r/B} = \mathbf{F}_{A/r}$,
- $[\mathbf{T}_{r/B,P}]_{\mathcal{R}_r}(1:2) = [\mathbf{T}_{A/r,P}]_{\mathcal{R}_r}(1:2)$,
- $[\mathbf{T}_{r/B,P}]_{\mathcal{R}_r}(3) = -C_m$.

The TITOP model includes one additional input $i(t)$: the μ -step number (integer) and one additional output: θ . The angle θ is also the angular configuration of the input shaft of the gear box described in the next section.

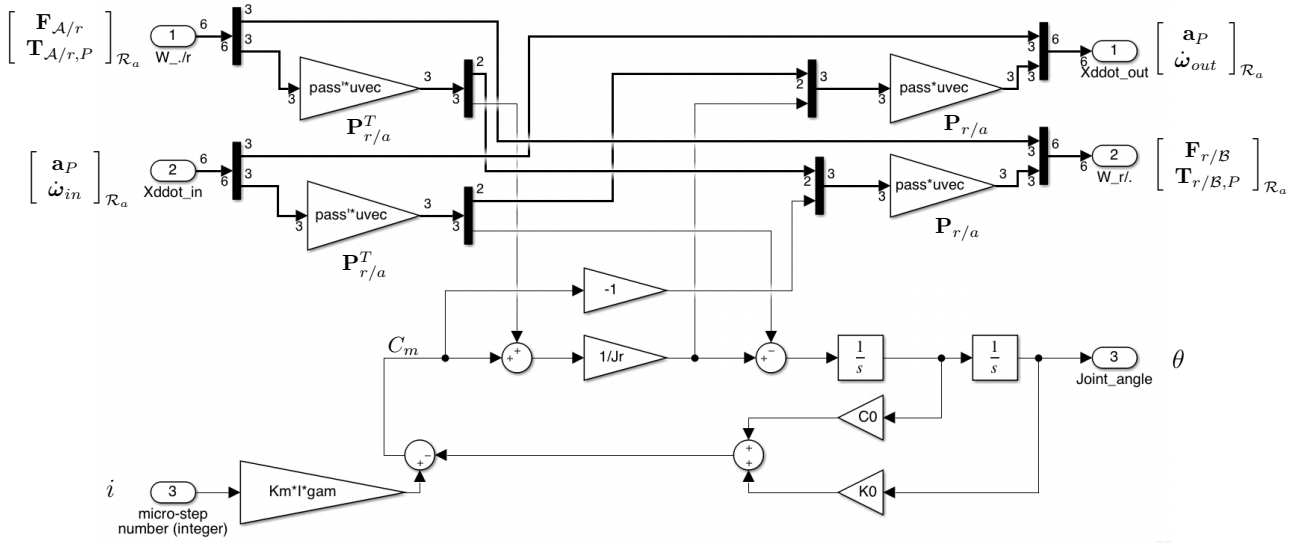


Figure 6: The block diagram representation of the TITOP model $M^r(s)$ of the stepper motor around \mathbf{r}_a in \mathcal{R}_a .

3.2 TITOP model $M^r(s)$ of the gearbox

It is also possible to define the TITOP model of the gear box in order to take into account:

- the two angular rates of the input (fast) and the output (slow) shafts,
- the disturbances torque due to contact imperfections in the gear pairs.

The gearbox model depends on the following parameters:

- N_g : the gearbox ratio,
- K_g and C_g : respectively stiffness and damping of the gearbox,
- J_o : inertia of the output shaft,
- J_i : inertia of the input shaft,
- \mathbf{r}_a : direction of the gear axis in load frame. The load is represented by the solar array (SA)

Let us denote:

- $T_{/o} = [\mathbf{r}_a]_{\mathcal{R}_a}^T [\mathbf{T}_{A/g,P}]_{\mathcal{R}_a}$ the torque applied by the SA on the output shaft of the gearbox at the connection point P around \mathbf{r}_a ,
- $T_{i/} = [\mathbf{r}_a]_{\mathcal{R}_a}^T [\mathbf{T}_{g/r,P}]_{\mathcal{R}_a}$ the torque applied by the input shaft of the gearbox to the stepper motor rotor at the connection point P around \mathbf{r}_a ,
- $\ddot{\theta}_o = [\mathbf{r}_a]_{\mathcal{R}_a}^T [\dot{\omega}_{out}]_{\mathcal{R}_a}$ the angular acceleration of the output shaft around \mathbf{r}_a .

- $\ddot{\theta}_i = [\mathbf{r}_a]^T_{\mathcal{R}_a} [\dot{\boldsymbol{\omega}}_{in}]_{\mathcal{R}_a}$ the angular acceleration of the input shaft around \mathbf{r}_a .

The angular deflection of the gearbox due to its stiffness, seen from the output shaft reads:

$$\delta\theta_o = \theta_o - \frac{\theta_i}{N_g} \quad (1)$$

and the internal reaction torque on the output shaft can be described by:

$$T_{g/o} = -K_g\delta\theta_o - C_g\delta\dot{\theta}_o + T_{pert}$$

where T_{pert} is an harmonic disturbance due to one or more contact imperfection(s) in gear pairs inside the gear box. The harmonic frequencies are characterized in the following paragraphs. Then, the dynamic model of the gearbox reads:

$$J_o\ddot{\theta}_o = T_{/o} + T_{g/o} \quad (2)$$

$$J_i\ddot{\theta}_i = -T_{i/} - T_{g/o}/N_g \quad (3)$$

The TITOP model $M^g(s)$ of the gearbox can be described by the block-diagram represented in Figure 7. Note that one can chose $J_i = 0$ to implement this model but $J_o \neq 0$.

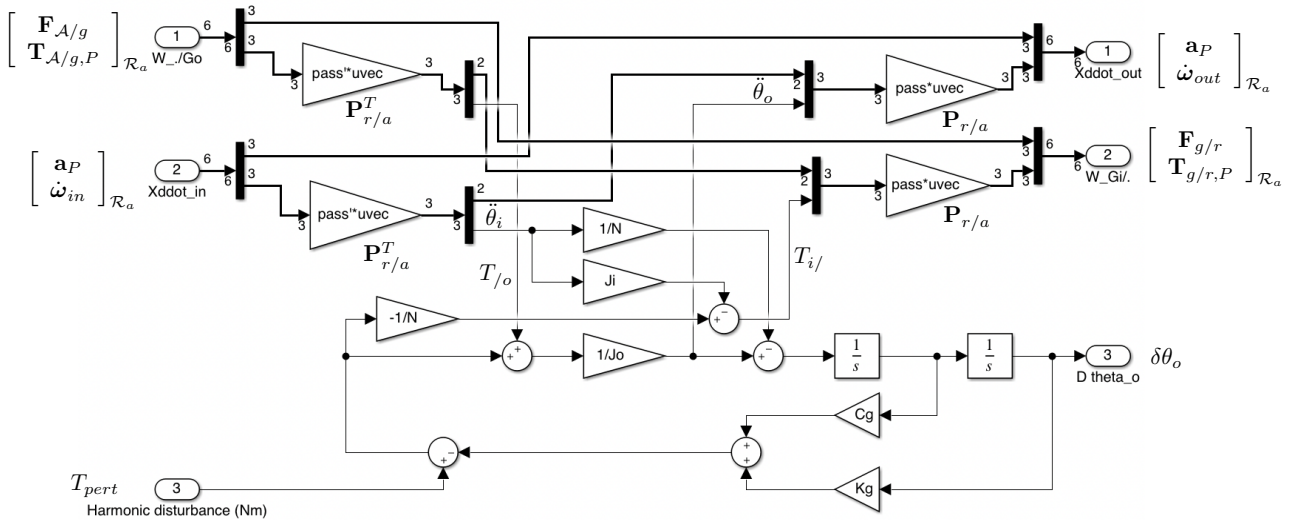


Figure 7: The block diagram representation of the TITOP model $M^g(s)$ of the gearbox around \mathbf{r}_a in \mathcal{R}_a .

Finally the disturbing torque T_{pert} can be characterized thanks to a previously developed toolbox ([5],[6]). This toolbox requires only the kinematic description of the mechanism as it is depicted in Figure 8 for the case of the considered SADM gearbox.

Then the toolbox can compute the angular rate of each body involved in the mechanism (see Table 2) and the frequencies ω_{d_i} of each contact imperfection i in the various gear pairs (see Table 3: $n_f = 6$

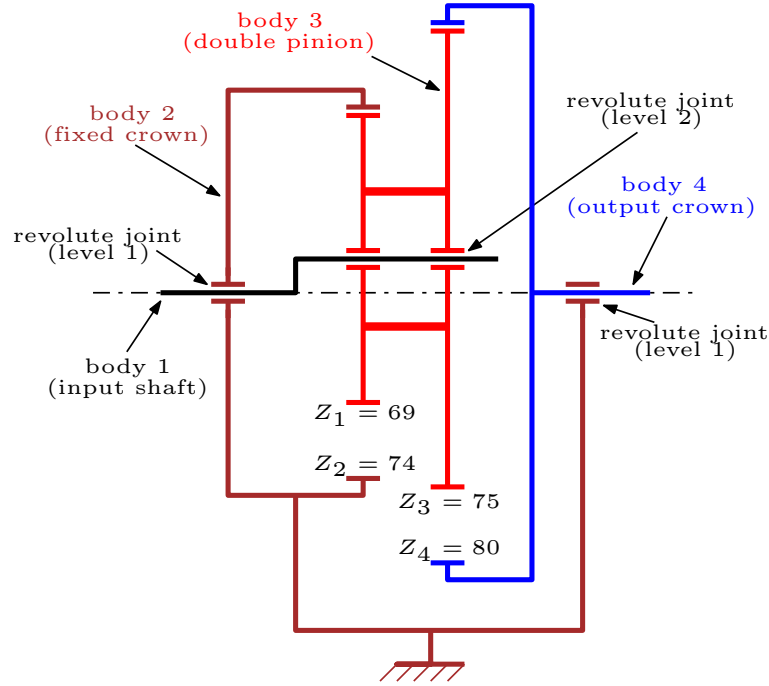


Figure 8: Kinematic model of the SADM gearbox (Z_i : gear teeth number).

contact frequencies can be identified in the SADM gearbox). Each imperfection i can create an harmonic disturbing torque $s_i(t)$ involving the fundamental frequency ω_{d_i} (rd/s) and $h_i - 1$ harmonics: $k\omega_{d_i}$ for $k = 2, 3, \dots, h_i$. The total disturbing torque T_{pert} at the input of the TITOP model $M^r(s)$ of the gearbox reads:

$$T_{pert}(t) = \sum_{i=1}^{n_f} \underbrace{\sum_{k=1}^{h_i} A_{i,k} \sin(k\omega_{d_i}t + \phi_{i,k})}_{s_i(t)}. \quad (4)$$

The magnitude $A_{i,k}$ and the phase $\phi_{i,k}$ of the k -th harmonic of the i -th imperfection depends of course on the shape of the imperfection. The simulation presented in Section 5 was obtained considering the contact imperfections # 2 and 3 with a saw-teeth profile or a narrow square profile (see Table (4)).

body $j =$	1	2	3	4
ω_j/ω_4	-184	0	13.33	1

Table 2: Body angular rates in the gearbox mechanism, normalized according to the output shaft (body 4).

4 ANALYSIS MODEL OF THE VALIDATION STUDY CASE

The study case is an operational European spacecraft composed of a main body (\mathcal{B}) and a flexible solar array (\mathcal{A}) defined by a NASTRAN[®] model. The SADM drives the solar pannel at a constant

imperfection $i =$	$\widetilde{\omega}_{d_i} = \omega_{d_i}/\omega_4$	gear pair	cause	number of sources
1	13616	(2,3)	gear frequency	1
2	184	(2,3)	a tooth on body 2	74
3	197.3	(2,3)	a tooth on body 3	69
4	14800	(3,4)	gear frequency	1
5	197.3	(3,4)	a tooth on body 3	75
6	185	(3,4)	a tooth on body 4	80

Table 3: Contact frequencies in the gearbox mechanism, normalized according to the output shaft (body 4) such that $\omega_4 = \omega_{SA}$.

	profile	$A_{i,k}$	$\phi_{i,k}$
saw-teeth		$-\frac{2a_i}{k\pi}(-1)^k$	0
dt - narrow square		$\frac{2a_i}{k\pi}(-1)^k (\cos(k dt \omega_{d_i}) - 1)$	0

Table 4: Harmonic magnitudes of typical profiles.

angular rate ω_{SA} ($\omega_{SA} = 0.06 \text{ deg/s}$).

The previous development are embedded in a SIMULINK[®] interface so that the model of the whole system can be assembled just by connection of the various subsystems, as it can be seen in Figure 9. This SIMULINK[®] model involves 4 subsystems:

- `u_HUB` (body) (white): the rigid main body \mathcal{B} with 2 ports (points): the ports `P1` (center of gravity: B) and `P2`, (the connection point P with the SADM),
- `2 phase stepper motor` (green): the TITOP model $M^r(s)$ of the stepper motor r with its own input # 1 (μ -step integer $i(t)$),
- `Gear Box` (g) (cyan): the TITOP model $M^g(s)$ of the gear box g with its own disturbing torque input # 2 (T_{pert} (Nm)),
- `u_SA` (body) (magenta): the flexible solar array \mathcal{A} taking into account the first 6 flexible modes provided by the NASTRAN[®] analysis output file. This model is plugged to the output shaft of the gear box through the 6×6 DCM matrix `6x6 v-rotation` (and its transposed `6x6 v-rotation'`) which is parameterized according to the angular configuration of the solar array (see appendix). In the nominal configuration the appendage frame \mathcal{R}_a is aligned on the main body frame \mathcal{R}_b .

A classical decentralized proportional derivative attitude control law (yellow) is tuned on the rigid model to have a given bandwidth (0.01 rd/s) on the three axis. This block diagram highlights also the definition of the different signals according to the notation proposed in the previous sections. Due to the mechanism located at point P , the acceleration twist is also referenced w.r.t. the considered body. For instance: $[\ddot{x}_P^g]_{\mathcal{R}_b}$ means the 6 dofs acceleration of point P on the output shaft of the gear box, projected in the main body frame..

The LPV model of the whole spacecraft is computed thanks to the function `ulinearize`. The frequency-domain response of the transfer from the 2 disturbances $i(t)$ and T_{pert} to the 3 pointing errors $[\phi, \theta, \psi]$ is depicted in Figure 10. It shows that the response to T_{pert} is 20dB higher than the response to $i(t)$. So the response to the stepper motor disturbance $i(t)$ will be no-more considered in the following parts. Furthermore the disturbance on $i(t)$ due to μ -step signal (integer) is a high frequency signal compared to the signal $s_i(t)$ due to an imperfection in the gearbox. Indeed, when the SADM drives the solar panel at a constant angular rate ω_{SA} , the ramp profile on the stepper motor angle, "angularly sampled" with μ -step value $\alpha = 0.125 \text{ deg}$ generates a disturbance which can be modeled by a saw-teeth signal depicted in Table 4. The frequency ω and the magnitude a of this signal are $\omega = \frac{2\pi|N|}{\alpha}\omega_{SA}$ and $a = \alpha/2$ ($N = -184$ is the gear-box ratio). Thus $\omega = 529920\omega_{SA}$: this frequency ratio is significantly higher than the gearbox imperfection frequency ratio depicted in Table 3.

Considering Table 3, it is clear that the gearbox imperfections are low frequency signals and they can excite the solar array flexible modes. That is highlighted on Figure 11 where the 14-th to 49-th harmonics (H14 to H49) of the imperfection #3 fundamental frequency are superposed to the mechanical system frequency-domain responses for various solar array angular configurations. From this Figure one can conclude that:

- H15 and H16 can interact with the first mechanical resonance (around 3.2 rad/s),

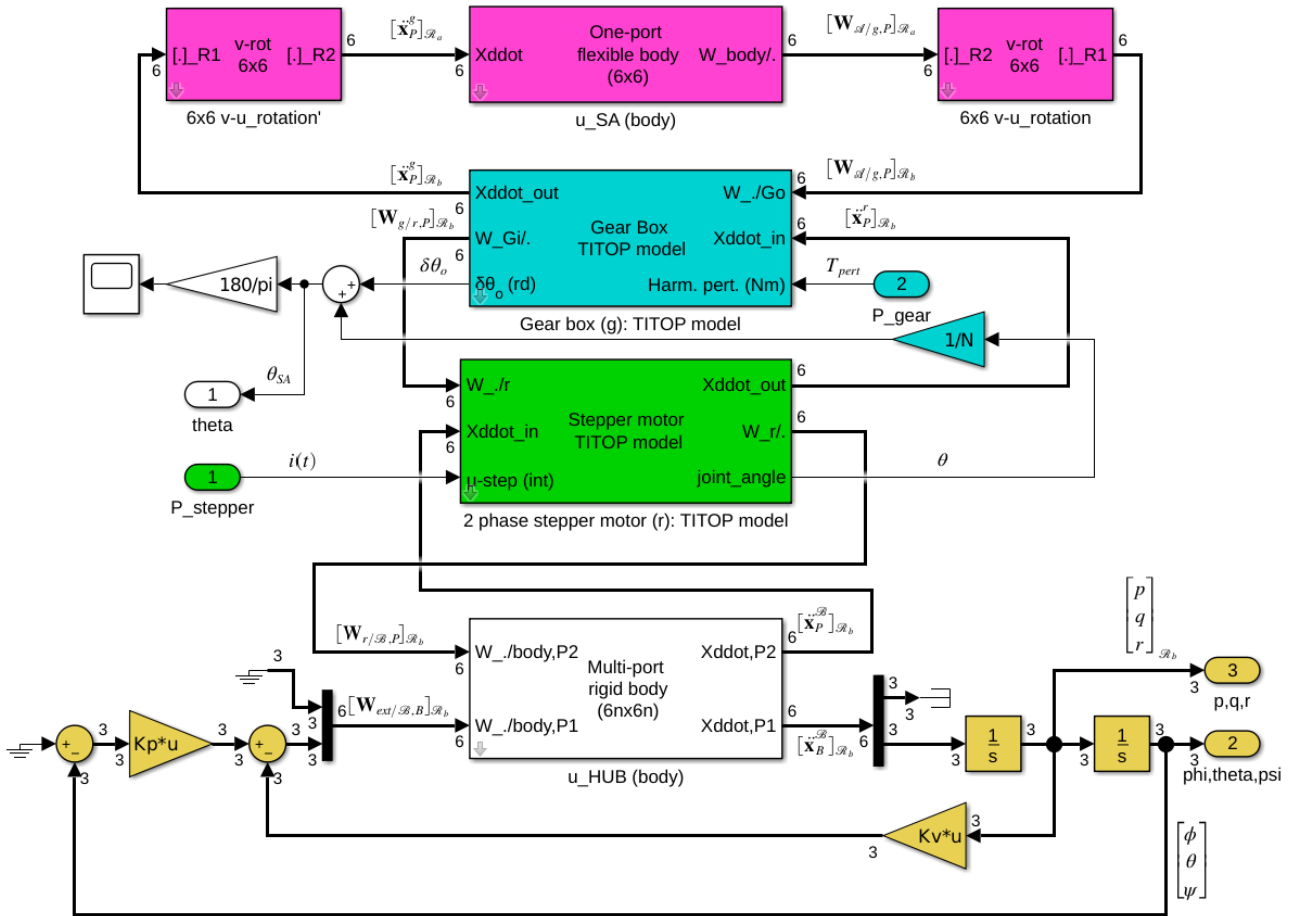


Figure 9: SIMULINK[®] analysis model of the generic Earth observation spacecraft.

- H22 to H25 can interact with the second mechanical resonance (around 5 rad/s),
- there are no harmonics which can interact with the third resonance (around 9.4 rad/s).

Due to the numerous possible imperfections in the gear box and their different harmonics a MATLAB[®] function `wcgainsfreqh`, based on μ -analysis, was developed to compute the worst case gain and the corresponding worst-case parametric configuration (the solar panel angular configuration in our case) for the various transfers of a MIMO system. This function can be used to find the worst-case gains g_{wc} , the worst-case solar array configurations θ_{wc} and the worst-case harmonics h_{wc} for a gear-box imperfection modeled with a particular profile (corresponding to a particular set of amplitudes) for its first N_h harmonics (see Table 4). For instance: for the gear box imperfections # 2, 3 and 6 modeled with the saw-teeth profile and $N_h = 60$, the obtained results are summarized in Table 5.

Conclusion: for the 3 considered gear-box imperfections, the worst-case appears on the mechanical resonance around 5 rd/s (2-nd flexible mode of the solar array, see Figure 11). Note also that the results presented in Table 5 are consistent with the spectral contributions computed from telemetries and presented in the next section.

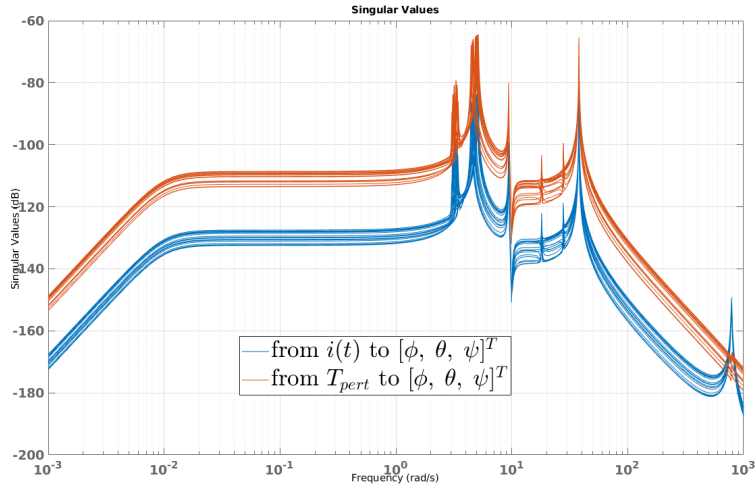


Figure 10: Frequency-domain response from disturbances to pointing errors.

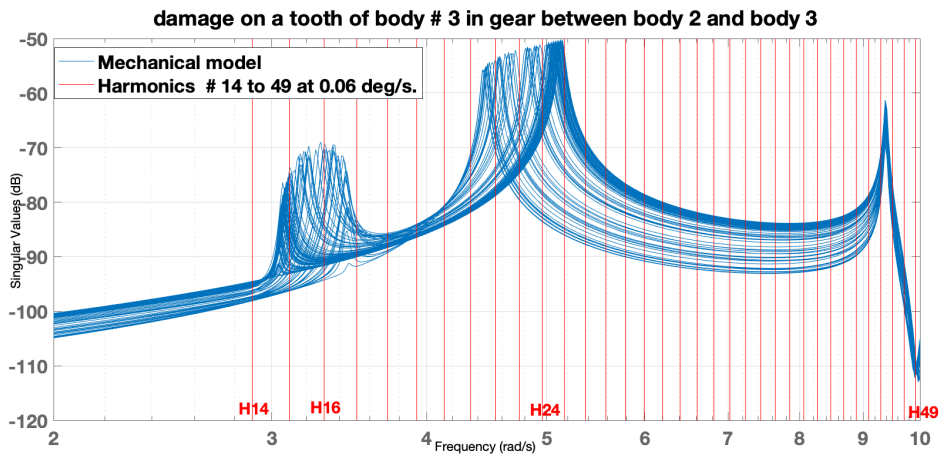


Figure 11: Frequency-domain response between gear disturbance T_{pert} and angular rates p , q , r and interaction with the harmonics $H14$ to $H49$ of imperfection #3 .

5 SIMULATION MODEL AND RESULTS

Due to the numerous algebraic loops in the SIMULINK[®] analysis model (Figure 9), the simulation is too much time consuming (around 8 hours to simulate the 3600 s) and this model will not be used any more. For simulation purpose it is highly recommended to evaluate this LPV model on a grid of the scheduling parameter $\sigma_4 = \tan(\theta_{SA}/4)$ (for instance with a step of one degree on θ_{SA}). The set of models thus obtained can then be stocked in array of LTI models, named `sysLPV`. The SIMULINK[®] block from the Control toolbox `LPV system` can then be used to simulated the LPV model with θ_{SA}

imperfection #	$2, \omega_{d_2} = 0.1927 \text{ rd/s}$			$3, \omega_{d_3} = 0.2066 \text{ rd/s}$			$6, \omega_{d_6} = 0.1937 \text{ rd/s}$		
	g_{wc}	θ_{wc}	h_{wc}	g_{wc}	θ_{wc}	h_{wc}	g_{wc}	θ_{wc}	h_{wc}
p	69.6	-119	26	71.0	-126	24	63.8	-136	25
q	1.26	-177	23	1.35	-161	22	1.43	-174	23
r	42.1	-177	23	41.3	-161	22	32.3	-173	24

Table 5: Worst case gains (g_{wc} $\mu\text{rad}/N/m/s$), SA angular configurations (θ_{wc} deg) and harmonics (h_{wc}) for the imperfections #2, #3 and #6 identified in Table 3 and modeled as saw-teeth signals.

(the first output of the model) as scheduling parameter. The SIMULINK[®] file is shown in Figure 12.

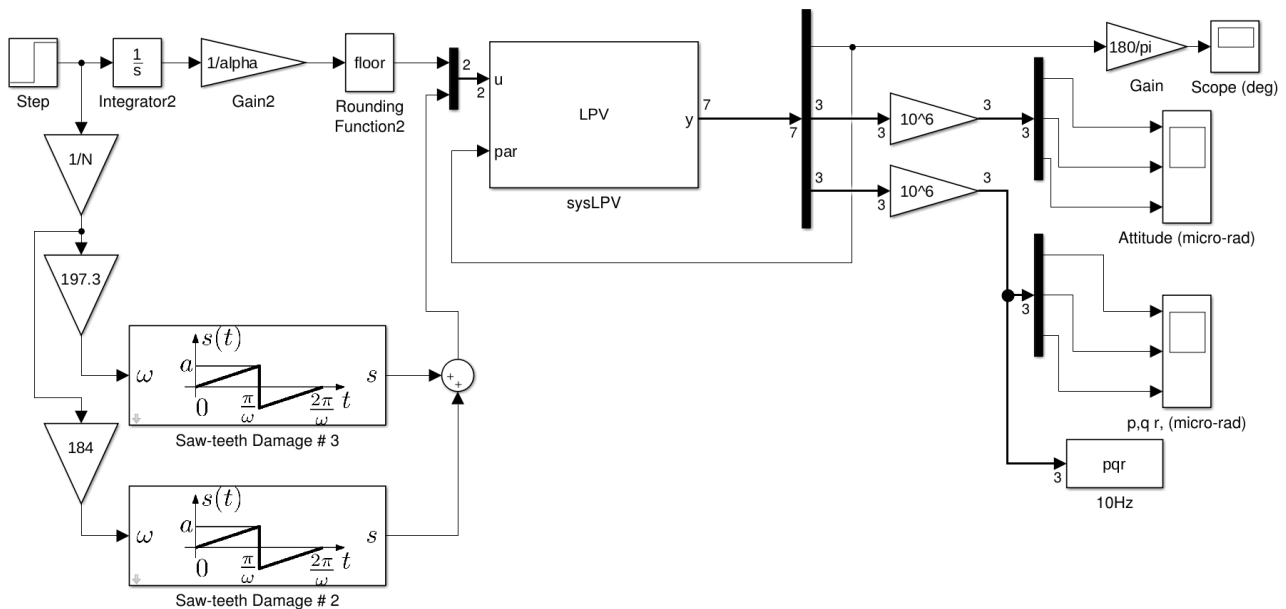


Figure 12: SIMULINK model for simulation.

The response of the 3 angular rates is depicted in Figure 13 (over 3600 s). This simulation was obtained considering the imperfections # 2 and 3 (see Table 3), modeled as saw-teeth signal with a magnitude $a = 0.5 \text{ Nm}$. This simulation highlights, in the time-domain, the excitation of SA flexible modes for particular angular configurations as it was noticed on the tele-measurements.

6 CONCLUSION AND PERSPECTIVES

This paper presents a dynamic model of a flexible spacecraft with an accurate model of a local mechanism (SADM) in order to perform deep analysis of pointing errors due to the mechanism internal disturbances. This approach was successfully applied on an Earth observation spacecraft and validated thanks to the recorded telemetries. The developed model allows to predict where is located the most

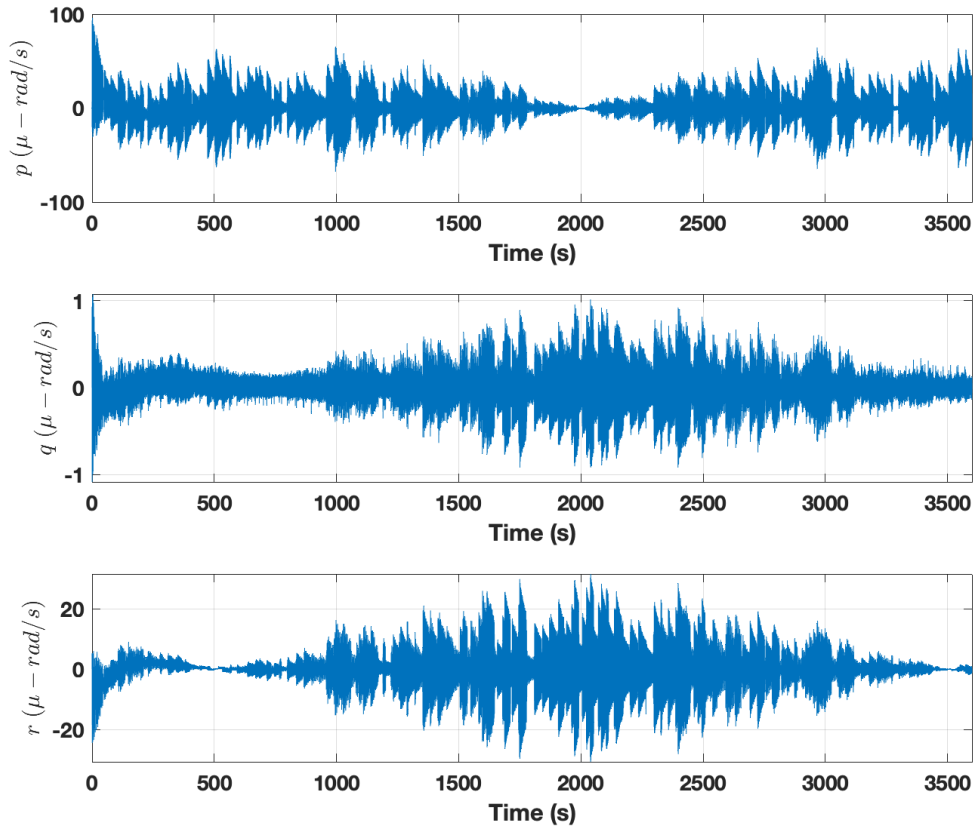


Figure 13: Time-domain response of the satellite angular rates.

critical imperfection in the gearbox. This model will be used in further studies to develop an on-board estimator of the attitude pointing error.

REFERENCES

- [1] C. Cumer, D. Alazard, A. Grynadier, and C. Pittet, “Codesign mechanics / attitude control for a simplified aocs preliminary synthesis,” in *ESA GNC 2014 - 9th International ESA Conference on Guidance, navigation & Control Systems*, Porto, PT, 2014, pp. 1–9. [Online]. Available: <https://oatao.univ-toulouse.fr/13643/>
- [2] F. Sanfedino, D. Alazard, V. Pommier-Budinger, F. Boquet, and A. Falcoz, “Dynamic modeling and analysis of micro-vibration jitter of a spacecraft with solar arrays drive mechanism for control purposes,” in *ESA GNC, 29 May- 2 June 2017, Salzburg, Austria*, 2017.
- [3] D. Alazard and C. Cumer. (2011) *Satellite dynamics toolbox - principle, user guide and*

tutorials. [Online]. Available: <https://personnel.isae-superaero.fr/daniel-alazard/matlab-packages/satellite-dynamics-toolbox.html>

- [4] J. Chen and W. Cheng, “Research on the disturbance generated by a solar array drive assembly driving a flexible system,” *Journal of Theoretical and Applied Mechanics*, vol. 54, no. 3, pp. 1001–1012, 2016. [Online]. Available: <http://dx.doi.org/10.15632/jtam-pl.54.3.1001>
- [5] D. Alazard and J. Penaud. Gearbox kinematic modeling. [Online]. Available: <https://personnel.isae-superaero.fr/daniel-alazard/matlab-packages/gearbox-kinematic-modeling.html>
- [6] J. Penaud, D. Alazard, and A. Amiez, “Kinematic analysis of spatial geared mechanisms,” *Journal of Mechanical Design*, vol. 134, no. 2, pp. 21 009 –21 014, 2012. [Online]. Available: <https://oatao.univ-toulouse.fr/8075/>
- [7] J. Chebbi, V. Dubanchet, J. A. P. Gonzalez, and D. Alazard, “Linear dynamics of flexible multibody systems : a system-based approach,” *Multibody System Dynamics*, vol. 41, no. 1, pp. 75–100, September 2017, thanks to Springer editor. The definitive version is available at <http://www.springerlink.com> The original PDF of the article can be found at Multibody System Dynamics website: <http://link.springer.com/journal/11044>. [Online]. Available: <https://oatao.univ-toulouse.fr/16559/>
- [8] V. Dubanchet, “Modeling and control of a flexible space robot to capture a tumbling debris,” Ph.D. dissertation, Institut Supérieur de l’Aéronautique et de l’Espace, Polytechnique Montréal, 2016.
- [9] N. Guy, D. Alazard, C. Cumer, and C. Charbonnel, “Dynamic modeling and analysis of spacecraft with variable tilt of flexible appendages,” *Journal of Dynamic Systems, Measurement, and Control*, vol. 136, no. 2, p. 021020, 2014.
- [10] D. Alazard, J. A. Perez, C. Cumer, and T. Loquen, “Two-input two-output port model for mechanical systems,” ser. AIAA SciTech. American Institute of Aeronautics and Astronautics, Jan 2015, 0. [Online]. Available: <http://dx.doi.org/10.2514/6.2015-1778>
- [11] H. Murali, D. Alazard, L. Massotti, F. Ankersen, and C. Toglia, “Mechanical-attitude controller co-design of large flexible space structures,” in *Advances in Aerospace Guidance, Navigation and Control*, J. Bordeneuve-Guibé, A. Drouin, and C. Roos, Eds. Springer International Publishing, 2015, pp. 659–678. [Online]. Available: http://dx.doi.org/10.1007/978-3-319-17518-8_38
- [12] F. Sanfedino, D. Alazard, V. Pommier-Budinger, A. Falcoz, and F. Boquet, “Finite element based n-port model for preliminary design of multibody systems,” *Journal of Sound and Vibration*, vol. 415, pp. 128–146, February 2018, thanks to Elsevier editor. The original PDF of the article can be found at <http://www.sciencedirect.com/science/article/pii/S0022460X17307915>. [Online]. Available: <https://oatao.univ-toulouse.fr/19279/>

- [13] C. Hervás García, I. Cantiello, G. Monroig, and E. Palombo, “Mechanism disturbance analysis. an approach to simplified rigid multibody dynamics,” in *ESA GNC, 29 May- 2 June 2017, Salzburg, Austria*, 2017.
- [14] Newton - Euler equations. [Online]. Available: https://en.wikipedia.org/wiki/Newton-Euler_equations
- [15] D. Alazard, C. Cumer, and K. Tantawi, “Linear dynamic modeling of spacecraft with various flexible appendages and on-board angular momentums,” in *7th International ESA Conference on Guidance, Navigation & Control Systems (GNC 2008)*, Tralee, IE, 2008, pp. 1–14. [Online]. Available: <https://oatao.univ-toulouse.fr/1899/>
- [16] J. A. P. Gonzalez, D. Alazard, T. Loquen, C. Pittet, and C. Cumer, “Flexible multibody system linear modeling for control using component modes synthesis and double-port approach,” *Journal of Dynamic Systems, Measurement, and Control*, vol. 138, no. 12, p. 121004, December 2016. [Online]. Available: <https://oatao.univ-toulouse.fr/16566/>
- [17] N. Guy, D. Alazard, C. Cumer, and C. Charbonnel, “Dynamic modeling and analysis of spacecraft with variable tilt of flexible appendages,” *Journal of Dynamic Systems Measurement and Control*, vol. 136, no. 2, January 2014. [Online]. Available: <https://oatao.univ-toulouse.fr/11016/>
- [18] —, “Modelling of satellite dynamics with uncertainties,” in *ESA GNC 2011 - 8th International ESA Conference on Guidance, navigation & Control Systems*, Carlsbad, Czech Republic, 2011.
- [19] J. Biannic and C. Roos. Generalized state-space: a new matlab class to model uncertain and non-linear systems as linear fractionar transformations. [Online]. Available: <https://w3.onera.fr/smac/>

APPENDIX: LPV MODEL ACCORDING TO THE ANGULAR CONFIGURATION

Let us define $\mathbf{P}_{a+\theta/a}$ as the DCM between the appendage frame $\mathcal{R}_{a+\theta}$ after a rotation of θ around r_a -axis and the initial appendage frame \mathcal{R}_a , i.e. (for a given vector \mathbf{v}):

$$[\mathbf{v}]_{\mathcal{R}_a} = \mathbf{P}_{a+\theta/a}[\mathbf{v}]_{\mathcal{R}_{a+\theta}}$$

with:

$$\begin{aligned} \bullet \mathbf{P}_{a+\theta/a} &= \mathbf{P}_{r/a} \begin{bmatrix} \cos \theta & -\sin \theta & 0 \\ \sin \theta & \cos \theta & 0 \\ 0 & 0 & 1 \end{bmatrix} \mathbf{P}_{r/a}^T, \\ \bullet \mathbf{P}_{r/a} &= \mathbf{P}_{r_a} \begin{bmatrix} \det(\mathbf{P}_{r_a}) & 0 & 0 \\ 0 & 1 & 0 \\ 0 & 0 & 1 \end{bmatrix}, \end{aligned}$$

- $\mathbf{P}_{r_a} = [\ker([\mathbf{r}_a]_{\mathcal{R}_a}^T) \quad [\mathbf{r}_a]_{\mathcal{R}_a}]$.

It is possible to define a LPV (Linear Parameter Varying) model of the system valid $\forall \theta \in [-\pi, +\pi]$, using the new parameter $\sigma_4 = \tan \frac{\theta}{4} \in [-1, 1]$. Indeed, the trigonometric relations [8]:

$$\cos \theta = \frac{(1 + \sigma_4^2)^2 - 8\sigma_4^2}{(1 + \sigma_4^2)^2}, \quad \sin \theta = \frac{4\sigma_4(1 - \sigma_4^2)}{(1 + \sigma_4^2)^2}$$

allows to define the block diagram representation of $\mathbf{P}_{a+\theta/a}$ depicted in Figure 14 where the varying parameter σ_4 can be declared using the MATLAB function `ureal` of the Robust Control Toolbox. Then, the MATLAB function `linearize` allows to compute an LFT representation of the system and gives access to all the tools of the Robust Control Toolbox.

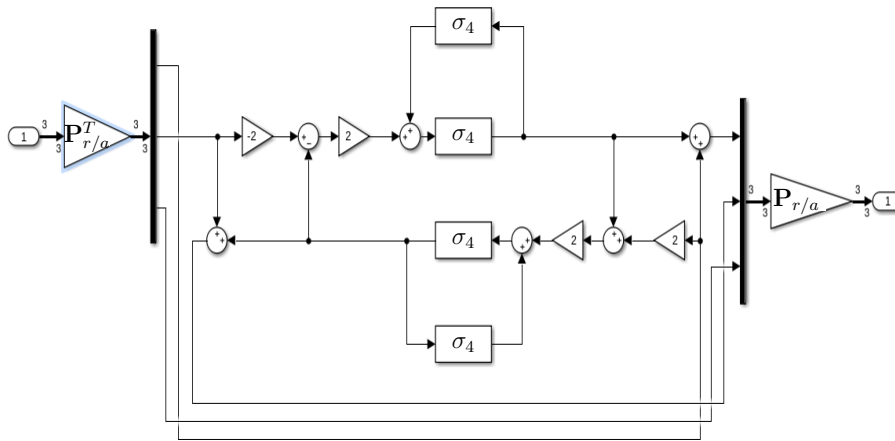


Figure 14: The block diagram representation of $\mathbf{P}_{a+\theta/a}$ parameterized with $\sigma_4 = \tan \frac{\theta}{4}$.